Determination of Structure and Effective Elastic Lithospheric Thickness of Ridge Belts. Zachary W. Williams[1], Paul K. Byrne[1], and Jeffrey A. Balcerski[2]. [1]Planetary Research Group, Department of Marine, Earth, and Atmospheric Sciences, North Carolina State University, Raleigh, NC 27695 (zwwillia@ncsu.edu), [2]Ohio Aerospace Institute, Cleveland, OH 44142.

Introduction: Widely distributed within Venus' lowlands are linear to arcuate, positive-relief systems of shortening structures termed ridge belts [1–7]. Although these landforms have been recognized for some time, the relatively recent availability of regional topography at resolutions greater than the Magellan altimetry dataset [8] enables the structure of ridge belts to be studied in finer detail. Additionally, the improved vertical resolution of these data [8] allows for construction of computational models with which to estimate the geometry of thrust faults underlying Venus' ridge belts.

For this study, we mapped the tectonic structures—faults and folds—that comprise a globally distributed set of ridge belts, and characterized the observed deformation. We then used topographic profiles to acquire estimates for the local effective elastic lithospheric thickness, and fault penetration depth, at each ridge.

Data and Methods: We utilized global Magellan synthetic aperture radar (SAR) full-resolution radar map (FMAP) 75-meter-per-pixel (m/px) left- and right-look mosaics for the mapping portion of this study. For topographic measurements, we employed stereo-derived digital elevation models (DEMs) produced by Herrick et al. [8], which offer ~20% global coverage at 1–3 km/px resolution.

Fault Mapping: Identification and mapping of faults was conducted with the left- and right-look SAR survey global mosaics at 1:200,000 view scale for six ridge belts (with an example shown in **Fig. 1a**). Assuming a similar surface mineralogy across each belt, the variation in backscatter (that value gathered by SAR) is a function of surface roughness and incidence angle [9]. Radar-bright lineations are thus interpreted as alterations in topography due to faulting.

On the basis of comparison with tectonic structures on Earth and other rocky bodies, we interpreted arcuate fault traces as denoting shortening structures (likely folds atop thrust faults) [10]. Linear fault traces, commonly offset in an *en echelon* manner, were taken to correspond to normal faults. The ridge belts in this analysis are oriented orthogonally to the Magellan radar look-directions and are covered by both left- and right look SAR datasets. Therefore, the radar look direction in which a lineation is most prominent corresponds to the facing direction of the steeper fore limb and, by inference, the transport direction of the thrust fault.

Lithospheric Flexure: Twenty cross-sectional profiles were drawn across each ridge belt within the Herrick et al. DEMs [8] at ~20 km intervals. These profiles were reviewed for topographic signals indicative of flexure of the elastic lithosphere in response to the mass of the ridge belt, treating the belt as a line load akin to a seamount chain [11]. We identified five ridge belts (additional to those we structurally mapped) that display evidence for having downflexed their supporting lithosphere (**Fig 2**). The solution to the topographic response to a line load (represented as a point load on a one-dimensional profile), w, is given by the dampened sinusoidal function [11]:

$$w = w_0 e^{-\frac{x}{a}}\left(\cos\left(\frac{x}{a}\right) + \sin\left(\frac{x}{a}\right)\right), \quad [1]$$

where w_0 is the maximum amplitude of flexure along the breadth of the profile, x, with respect to the flexural parameter, a, given by the relation:

$$a = \sqrt[4]{\frac{4D}{(\rho_m - \rho_i)g}}. \quad [2]$$

Here, D is the flexural rigidity, $\rho_m - \rho_i$ is the difference between mantle and atmospheric density, and g is the acceleration due to gravity. Flexural rigidity is given by

$$D = \frac{E}{12(1-\nu^2)}h^3, \quad [3]$$

where E is Young's modulus, ν is Poisson's ratio, and h is the thickness of the elastic lithosphere. Values for Young's modulus and Poisson's ratio for anhydrous basalt, and the density contrast across the lithosphere, were taken from previous studies of lithospheric flexure on Venus [12, 13]. The elastic lithosphere thickness was found with a least-squares optimization of a cost function for the set of equations using a simplex method, with h and w_0 as two of the free parameters.

Elastic Dislocation Modeling: Shear failure—that is, faulting—is restricted to rock that behaves in a brittle manner, and which occurs only in the upper crust. Therefore, the maximum penetration depth of faulting provides a *minimum* value for the depth to the brittle–ductile transition (BDT), placing constraints on the mechanical structure of the crust in which the ridge belts have formed [14–17]. We thus determined the geometry and penetration depth of the major thrust fault planes beneath the six ridge belts we structurally mapped with the Coulomb 3.3 elastic dislocation software.

We created a suite of user-defined fault geometries that iterated through a parameter space of possible slip amounts, dip angles, and vertical and horizontal coordinates of a given belt's underlying fault plane. We considered several input fault–fold geometries, including fault-bend folds, fault-propagation folds, and listric

thrust faults within our parameter space. Elastic dislocation solutions [18] to these inputs yielded a stress state and resulting deformation of the model grid in two dimensions (along the X–Z axes). Our models were iteratively refined to produce best-fit solutions as defined by the normalized root-mean square error (RMSE) between modeled surface deformation and cross-sectional profiles taken earlier in this study. We regarded model solutions with an RMSE value below 0.2 to give acceptable fits and thus estimates for the maximum penetration depth of the major thrusts under each ridge belt (and depth *minima* for the BDT at the time of ridge belt formation).

Results and Discussion: *Fault Analysis:* Our mapping and morphological analyses confirm that tectonic structures within ridge belts are predominately thrust faults and their related folds, the majority of which strike roughly parallel with the long axis of the host ridge belt itself (**Fig. 1a**). The cumulative lengths of fault populations, discretized by dip-direction, were compared within a given ridge belt to determine if a dominant fault dip direction is present within that belt. This analysis yielded a direction of tectonic transport consistent with that suggested by the fore- and backlimb morphology seen in topographic profiles in the four ridge belts included in this study that displayed such cross-sectional asymmetry.

Thrusts within the ridge belts commonly form antithetic pairs and imbricated anticlines (**Fig. 1b**), the distances between which may offer information regarding homogeneity in slip and fault dip angle along major underlying fault planes [19]. The spacing distribution of surface anticlines varies among the ridge belts we considered. We interpret this spatial variation to reflect heterogeneities in the mechanical properties of the major faults comprising these ridge belts, likely influenced by variations in lithology. We thus regard ridge belts as complex systems of thrust fault duplexes, in contrast to shortening structures on other worlds that are often morphologically more simple, such as the "lobate scarps" on Mercury and Mars.

Model Solutions: Our assessment of the thickness of the elastic lithosphere from downflexing by the ridges returned values of 4–24 km (**Fig. 2**). Coulomb elastic dislocation best-fit solutions all feature a listric fault plane rooting to a detachment zone with depths ranging 14–29 km. (**Fig. 3**). The value ranges returned by both of these approaches—in total, from 4 to 29 km—agrees with previous findings that the elastic lithosphere in the Venus lowlands is relatively thin in comparison to the crusts of other terrestrial planets. [13, 20–22].

References: [1] Frank, S. L. and Head, J. W. III. (1990) *EMP.* [2] Ivanov, M. A. and Head, J. W (2013) *PSS, 84.* [3] Barsukov, V. L. et al. (1986) *JGR, 91.* [4] McGill, G. E. and Campbell, B. A. (2006) *JGR, 111.* [5] Ivanov, M. A. and Head, J. W. (2011) *PSS, 59.* [6] Solomon, S. C. et al. (1992) *JGR, 97.* [7] Basilevsky, A. T. and Head, J. W. (2003) *Report on Progress in Physics, 66.* [8] Herrick, R. R. et al. (2012) *EOS, 93, No. 12.* [9] Farr, T. G. (1993) *Guide to Magellan Image Interpretation.* [10] Burg, JP. (2017) *Tectonics: Thrust Systems.* [11] Lowrie, W. (2007) *Fundamentals of Geophysics.* [12] O'Rourke, J. G. and Smrekar, S. E. (2018) *JGR, 123.* [13] Anderson, F. S. and Smrekar, S. E. (2006) *JGR, 111.* [14] Balcerski, J. A. and Byrne, P. K. (2018) *VEXAG 2018,* abstract 2137. [15] Peterson et al. (2020) *JGR, 125.* [16] Shultz and Watters. (2001) *GRL, 28.* [17] Byrne, P.K. et al. (2015) *EPSL, 427.* [18] Okada, Y. (1992) *Seismological Society of America, 82.* [19] Schultz, R.A (1993) *JGR, 98.* [20] James, P.B. et al. (2012) *JGR, 118.*[21] Buck, W.R. (1992) *GRL, 19.* [22] Ghail, R. (2015) *PSS, 113-114.*

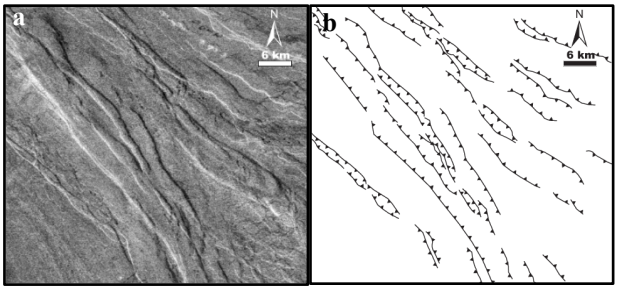

Fig. 1a. Folds observed within left- and right-look SAR (with right-look inverted) at 1:200,000 view scale. **b.** Structural map of faults, which commonly form antithetic pairs bounding anticlinal folds. Teeth indicate inferred fault down-dip direction.

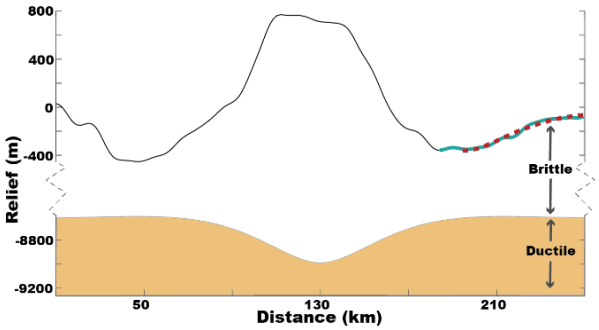

Fig. 2. An exemplar topographic profile of a ridge belt displaying evidence for lithospheric flexure (note the troughs at ~50 km and 170 km from the origin). An analytical solution to flexure, seen on the right side of the profile, returns an elastic thickness estimate of 9 km (with a normalized RMSE of 0.07).

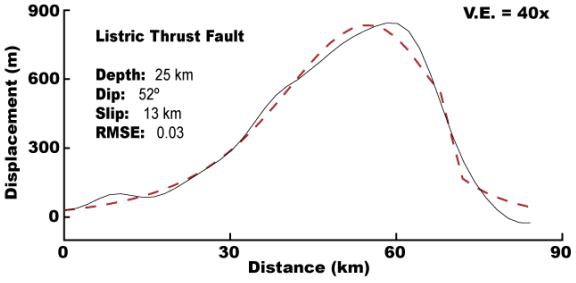

Fig. 3. Observed surface deformation of a ridge belt (solid black line) and forward modeled best-fit result (dashed red line) with a vertical exaggeration (V.E.) of 40. All best-fit results in this study feature slip tapering to zero along a listric fault plane (not shown here).